Supplementary Information

Nano-second timescale high-field phase transition in hydrogenated amorphous silicon

Rajat Sinha[1, 2, a)], Prasenjit Bhattacharya[3], Sanjiv Sambandan[3,4], and Mayank Shrivastava[1, b)]

[1)] Department of Electronic Systems Engineering, Indian Institute of Science, Bangalore 560012, India
[2)] Centre for Nano Science and Engineering, Indian Institute of Science, Bangalore 560012, India
[3)] Instrumentation and Applied Physics, Indian Institute of Science, Bangalore 560012, India
[4)] Department of Engineering, University of Cambridge, Cambridge, UK

[a)] rajats@iisc.ac.in
[b)] www.mayank.dese.iisc.ac.in

1. Nanosecond Pulse characterization setup

A. Pulse generation: The pulse generation setup used here, generates high voltage level pulses at very high frequencies and thus has to overcome the following challenges: 1. Generation of high amplitude pulses with proper pulse shaping 2. At very high frequencies, wavelength of the electrical signal is very high and can reach up the length of various parts of testing setup. Due to these issues, a conventional setup cannot be used to generate and transmit these pulses. Keeping this in mind, a different strategy is employed to generate these fast rising signals at timescales of nanoseconds. The signals are generated using two 50 Ω matched transmission lines connected through a mechanical reed switch (shown in fig.S1). At t<0, the transmission line L_1 is charged at a voltage level V_o. As soon as the switch is closed at t=0, the voltage at switch drops down to $V_o/2$ and voltage waves with the amplitude $V_o/2$ propagate in opposite directions at the switch ($-V_o/2$ reflection in L_1). After a certain time period, both the waves superimpose to provide a pulse of amplitude $V_o/2$, with the pulse width (PW) given by :

$$PW = \frac{2L}{v}$$

Where, 2L is the combined length of the lines L_1 and L_2 and v is the propagation velocity of the signal in the transmission line and depends on the relative permittivity of the transmission line material.

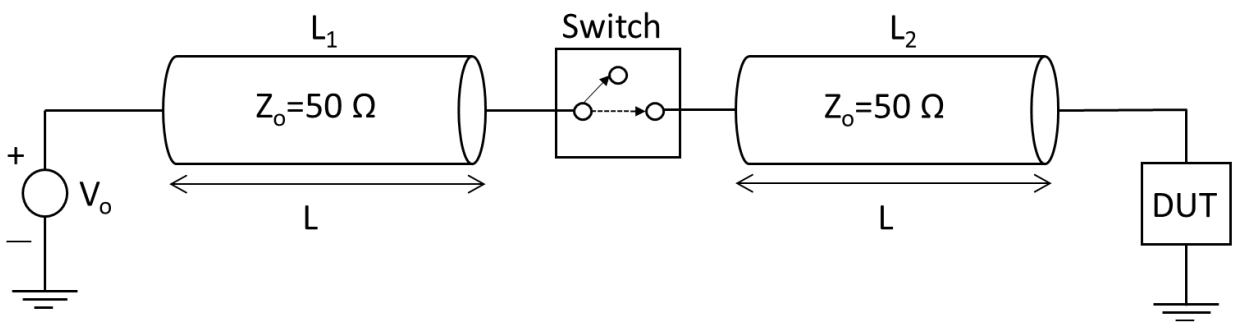

Fig.S1: Nano second time scales high amplitude pulse generation

B. Voltage and current measurement: Measurement cycle of a conventional source measurement unit lies in the range of a few hundred micro seconds and thus these units are not capable of measuring very high frequency current and voltage signals. To counter this issue, signals were captured using a high bandwidth oscilloscope (DPO 70404C from Tektronix). The device current was measured using a current sensor (basically a current transformer) CS-05VA with bandwidth >3GHz and sensitivity of 0.5mV/mA. The secondary coil of the sensor is terminated using a 50 Ω resistor, which converts current signals to corresponding voltage signals. Once the current and voltage waveforms are captured, these waveforms are averaged in a pre-defined averaging window (here 60-80%) and the resultant is used as a single value in quasi-static I-V characteristics. The averaging window is chosen in a time window, where the voltage and current waveforms are settled and there is no impact of fast rise and fall time (displayed in Fig.2b of the main text). Fig. S2 shows the oscilloscope along with the pulse generator used for capturing signals and generating electrical pulses respectively.

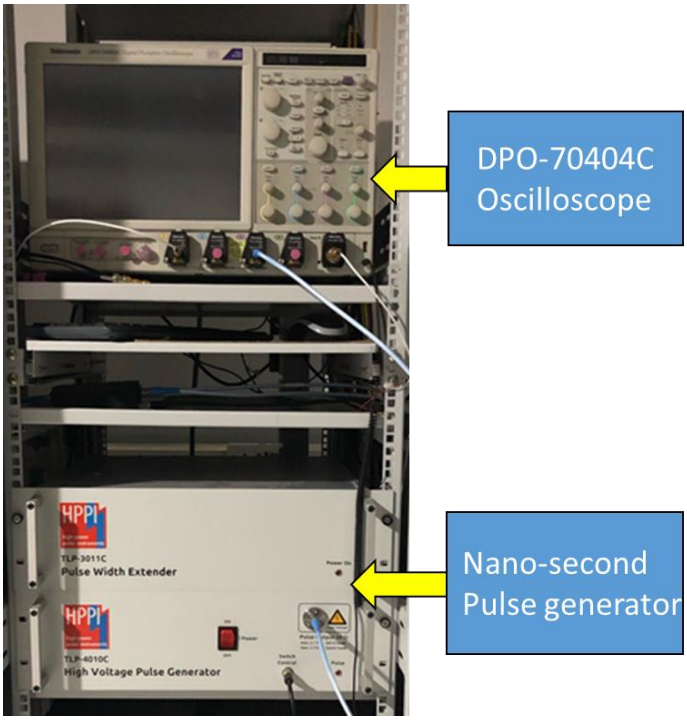

Fig.S2: Image showing the DPO-70404C Oscilloscope and nano-second pulse generator.

C. System Calibration: At high frequency dealt in this work, parasitic impedances of various lines and interfaces can play a highly detrimental role in measurement accuracy and pulse shape. To counter this issue, calibration of the entire setup was done against standard reference values. Calibration of the setup was done in the following sequence:

1. Time offsets in voltage and current channels was adjusted by applying a set of pulses across open metal pads. Electrical signals across open pads were also applied to measure effective resistance of the GS probes through which voltage across the device was captured.

2. Voltage channel was calibrated against the breakdown voltage of a reference surface mount Zener diode with a breakdown voltage of 32.10V.
3. Current channel was calibrated using a reference surface mount resistor of 99.716 Ω (shown in fig.S3).

D. Device Probing: The devices are probes using RF probes in 4-wire architecture. Probes with resistance of 5k Ω and 50 Ω were used on voltage sense and force side respectively. Probing was done inside a probe station with active vibration isolation.

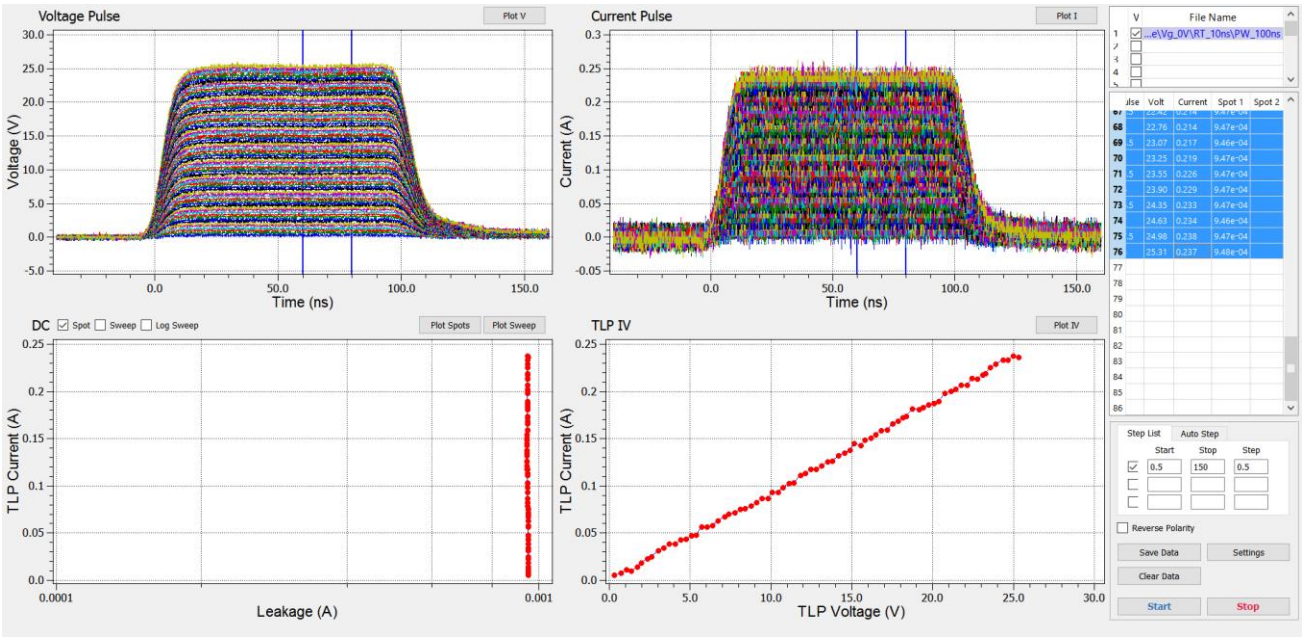

Fig.S3: Current and voltage waveforms, pulse I-V and low voltage DC results characteristics of a SMD resistor used for calibration. The voltage and current channels were calibrated prior to this. The pulse setup is controlled using a python based software.

2. Cross-sectional image of sample with silicon substrate

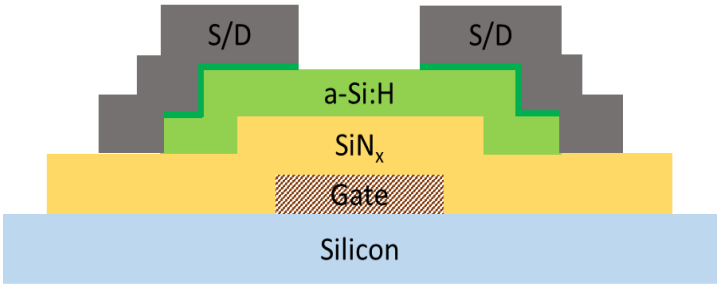

Fig S4: Cross-sectional view of the a-Si:H TFTs fabricated on silicon substrate.

3. EDS spectroscopy of a-Si:H samples

To further characterise the peaks observed in the AFM, energy dispersive x-ray spectroscopy was performed. Fig.S6 shows the SEM images with locations marked, where EDS was performed. Table S1 presents the elements present at different locations along with their composition.

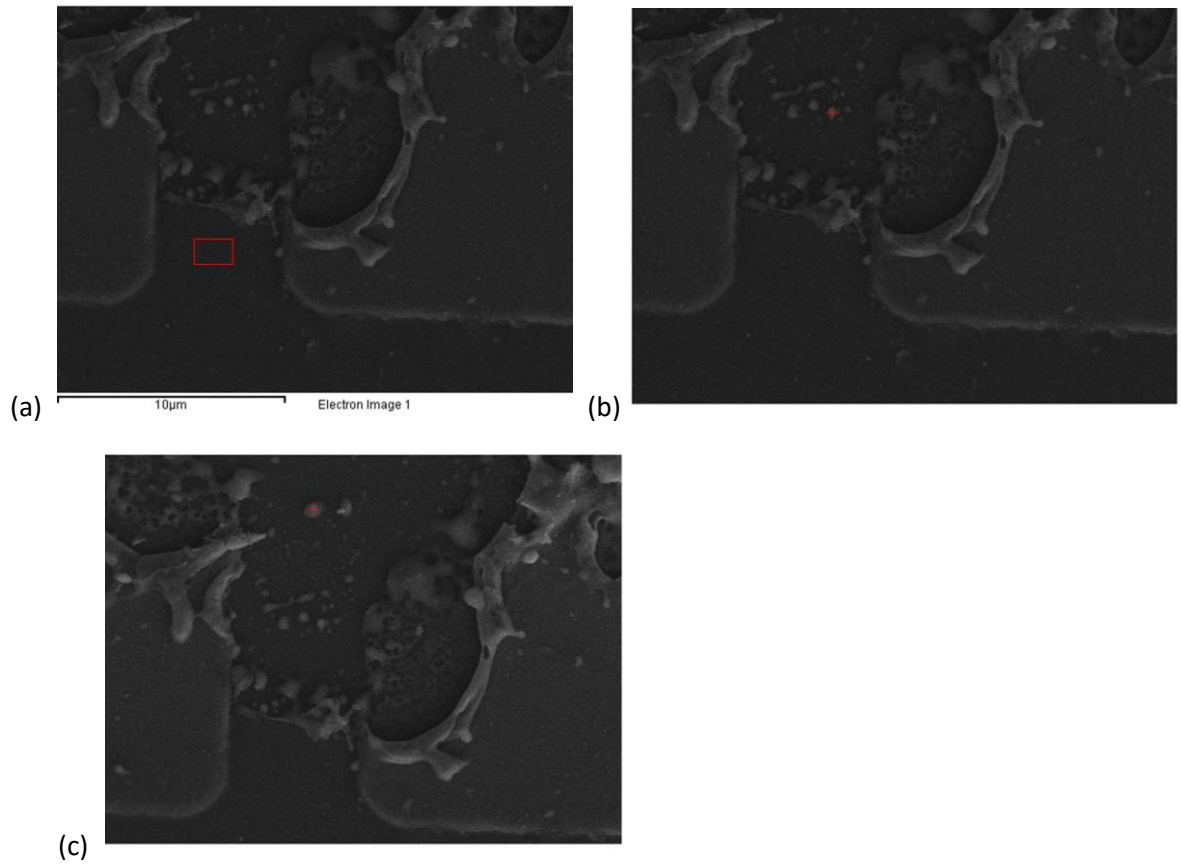

Fig. S5: SEM images depicting different locations where EDS spectroscopy was performed.

Location	Elements	Weight (%)
A	Aluminium	22.48
	Silicon	66.77
	Chromium	10.40
	Molybdenum	0.34
B	Nitrogen	0.74
	Aluminium	18.02
	Silicon	41.78
	Titanium	0.87
	Chromium	38.03
	Molybdenum	0.56
C	Aluminium	23.29
	Silicon	36.09
	Titanium	1.28
	Chromium	36.94
	Molybdenum	2.40

Table S1: Elements and their composition at different locations measured through EDS.

4. Deconvolution of the raman spectra of nc-Si.

Deconvolution of the Raman spectra of nc-Si (Fig. 3e in the main text) is done to provide information about the resultant nc-Si. The raman spectra is deconvoluted into three Gaussian peaks as shown in Fig.S4. The first component occurs at 480 cm^{-1} and is associated with the presence of amorphous component in the nc-Si. The second component occurs in the range of 511.8 cm^{-1} to 518.1 cm^{-1} and is associated with the nano crystalline component. The third component occurs in the range of 490.5 cm^{-1} to 507.7 cm^{-1} and is associated with the grain boundary effects[1]. Raman crystallization fraction (X_c) provides information about the fraction of crystalline component in the sample and is computed using the equation

$$X_c = \frac{I_c + I_{int}}{I_c + I_{am} + I_{int}}$$

Where I_c, I_{am} and I_{int} are the integrated intensities of crystalline, amorphous and grain boundary associated components[2]. X_c =0.51 for the sample. Bond angle deviation ($\Delta\theta$) is calculated using the equation

$$T^2 = (32)^2 + (6.75\,\Delta\theta)^2$$

Where T is the full width at half maxima of the amorphous component[3]. In the sample discussed, T is computed to be 55.5 cm^{-1}, which leads to $\Delta\theta$ being equal to 6.71°. The mean crystallite size is calculated using the equation

$$L_c = 2\pi \left(\frac{B}{\Delta\omega}\right)^{0.5}$$

Where B = 2 $cm^{-1}nm^2$ and $\Delta\omega$ is the shift of nano crystalline raman peak from that of c-Si[4]. L_c= 4.5nm.

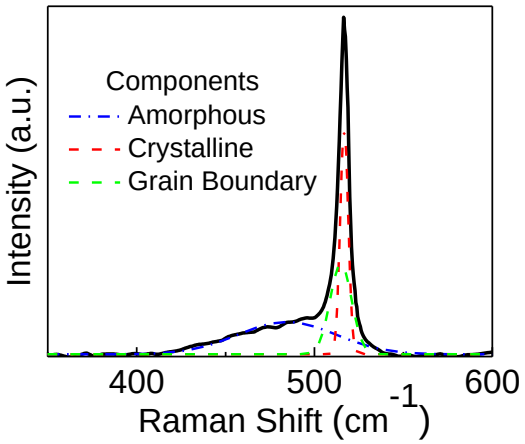

Fig.S6 Raman spectra of the device post phase transition showing a bump on the lower side of the raman shift along with the deconvoluted amorphous, grain boundary and nano crystalline components.

References

1. Veprek, S., Sarott, F. A., & Iqbal, Z. (1987). Effect of grain boundaries on the Raman spectra, optical absorption, and elastic light scattering in nanometer-sized crystalline silicon. *Physical Review B*, *36*(6), 3344.
2. Jana, M., Das, D., & Barua, A. K. (2002). Role of hydrogen in controlling the growth of μc-Si: H films from argon diluted SiH_4 plasma. *Journal of applied physics*, *91*(8), 5442-5448.
3. Tsu, R., Hernandez, J. G., & Pollak, F. H. (1984). Determination of energy barrier for structural relaxation in a-Si and a-Ge by Raman scattering. *Journal of Non-Crystalline Solids*, *66*(1-2), 109-114.
4. He, Y., Yin, C., Cheng, G., Wang, L., Liu, X., & Hu, G. Y. (1994). The structure and properties of nanosize crystalline silicon films. *Journal of Applied Physics*, *75*(2), 797-803.

5. Characterization of bond angle deviation and raman crystallization factor

Fig.S5 shows the variation of bond angle deviations and raman crystallisation factor of various points across the channel, which are nano-crystalline in nature (discussed in Fig.10 of main text). The source and drain contacts have similar orientation as in fig.10 of main text.

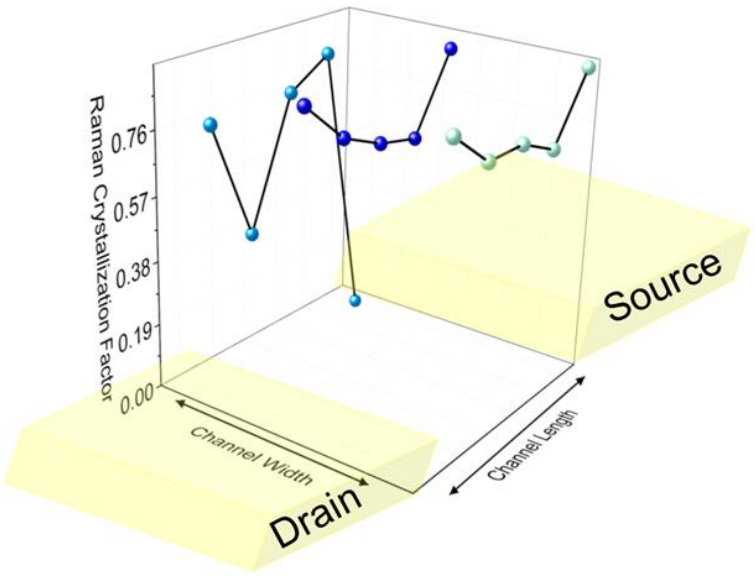

(a)

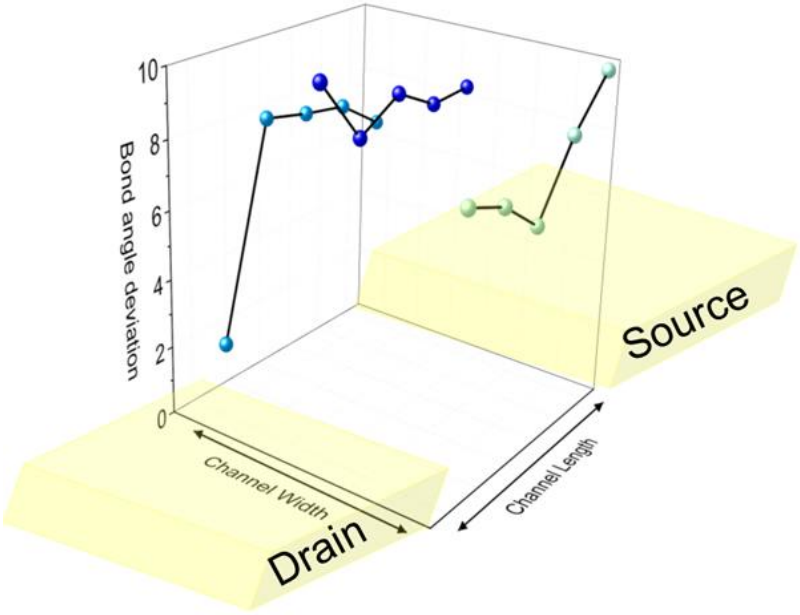

(b)

Fig S7. (a) Raman crystallization factor (b) Bond angle deviation for various points across the channel.

6. HRTEM images of the sample with [220] plane observed

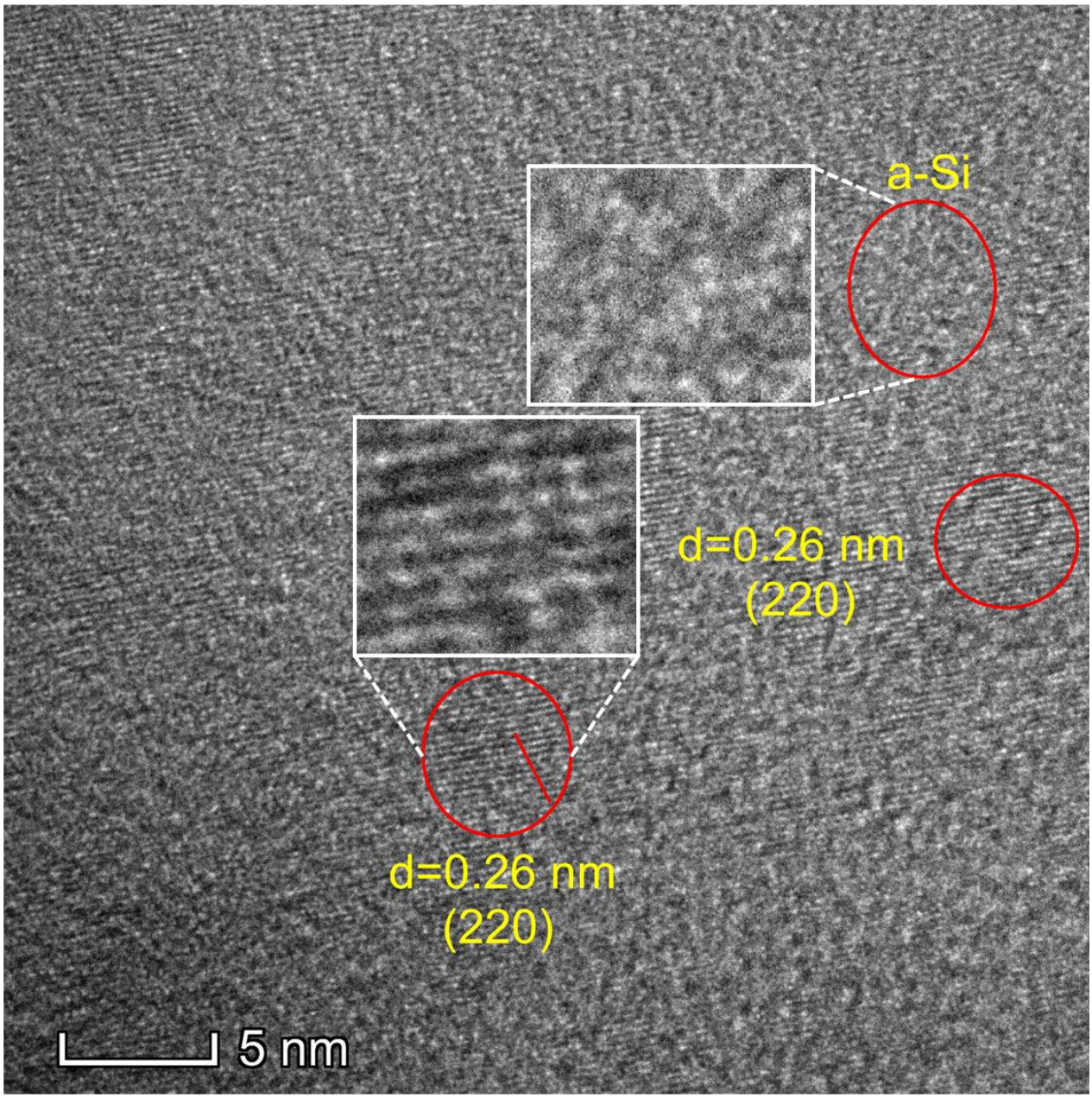

Fig S8: HRTEM image nc-Si post phase transition showing (220) plane.